INFERENCE ON ACCRETION FLOW DYNAMICS USING TCAF SOLUTION FROM THE ANALYSIS OF SPECTRAL EVOLUTION OF H 1743-322 DURING THE 2010 OUTBURST

Santanu Mondal[1], Dipak Debnath[1], and Sandip K. Chakrabarti[1,2]
[1] Indian Center for Space Physics, 43 Chalantika, Garia St. Road, Kolkata 700084, India; santanu@csp.res.in, dipak@csp.res.in, chakraba@bose.res.in
[2] S. N. Bose National Centre for Basic Sciences, Salt Lake, Kolkata 700098, India

ABSTRACT

We study accretion flow dynamics of the Galactic transient black hole candidate (BHC) H 1743-322 during its 2010 outburst by analyzing spectral data using the two-component advective flow (TCAF; Keplerian and sub-Keplerian) solution after its inclusion in XSPEC as a local model. We compare our TCAF solution fitted results with combined disk blackbody (DBB) and power-law (PL) model fitted results and find a similar smooth variation of thermal (Keplerian or DBB) and non-thermal (PL or sub-Keplerian) fluxes/rates in two types of model fits. For a spectral analysis, 2.5–25 keV spectral data from the *Rossi X-Ray Timing Explorer* Proportional Counter Array instrument are used. From the TCAF solution fit, accretion flow parameters, such as Keplerian rate, sub-Keplerian rate, location of centrifugal pressure-supported shock, and strength of the shock, are extracted, providing a deeper understanding of the accretion process and properties of accretion disks around BHC H 1743-322 during its X-ray outburst. Based on the halo to disk accretion rate ratio, shock properties, accretion rates, and the nature of the quasi-periodic oscillations' (if observed) entire outburst is classified into four different spectral states: hard, hard-intermediate, soft-intermediate, and soft. From the time variation of intrinsic flow parameters, it appears that their evolutions in the declining phase do not retrace the path of the rising phase. Since our current model does not include magnetic fields, spectral turnover at energies beyond 500–600 keV cannot be explained.

Key words: accretion, accretion disks – hydrodynamics – radiation: dynamics – shock waves – stars: black holes – stars: individual (H 1743-322)

1. INTRODUCTION

Galactic transient black hole candidates (BHCs) are very interesting objects to study because these sources generally show evolutions in their temporal and spectral properties during their outburst phases, which are strongly correlated to each other. In last two decades, especially after the launch of the *Rossi X-Ray Timing Explorer* (*RXTE*), our understanding of BHCs has progressed significantly, but not to the extent that we can visualize how the flow configuration and properties are changing within short timescales of less than a day. In general, it has been found that during outbursts of a BHC, four basic spectral states, namely, hard (HS), hard-intermediate (HIMS), soft-intermediate (SIMS), and soft (SS), are observed (see Nandi et al. 2012 and references therein). Detailed discussions on the evolution of the temporal and spectral properties of different BHCs during their outbursts were made by several groups (see, e.g., McClintok & Remillard 2006; Belloni et al. 2005; Nandi et al. 2012). Different branches of the hardness intensity diagram (HID; Maccarone & Coppi 2003; Belloni et al. 2005, etc.) are also related to different spectral states.

It is well established that a standard Keplerian disk (Shakura & Sunyaev 1973) cannot explain the full X-ray spectrum of BHCs, and one necessarily requires a second component, namely, the so-called Compton cloud (Sunyaev & Titarchuk 1980, 1985), to produce the power-law (PL) part of the spectrum. There are speculations regarding the origin and nature of this Compton cloud, which range from a magnetic corona (Galeev et al. 1979) to a hot gas corona over the disk (Haardt & Maraschi 1993; Zdziarski et al. 2003). Observational evidence shows that while both the components must be dynamic, one component moves faster (e.g., Smith et al. 2002; Soria et al. 2001; Wu et al. 2002; Cambier & Smith 2013), much like the low angular momentum, sub-Keplerian transonic flow component as incorporated in Chakrabarti & Titarchuk (1995, hereafter CT95). In the two-component advective flow (TCAF) solution, Chakrabarti and his collaborators, even before the *RXTE* was launched, envisaged that the Compton cloud is actually the inefficiently radiating transonic flow (Chakrabarti 1990) with very low or sub-Keplerian angular momentum. Matter in this accretion flow becomes hot close to the black hole where the centrifugal pressure starts dominating, and an accretion shock may or may not form depending on whether or not the Rankine–Hugoniot shock conditions are satisfied (CT95; Chakrabarti 1997, hereafter C97). Recently, Mondal & Chakrabarti (2013) and Giri & Chakrabarti (2013) showed that a self-consistent and stable transonic solution that supports the solution envisaged by CT95 exists.

The stellar mass BHC H 1743-322 is very intriguing because in the last decade after its re-discovery in 2003 (Revnivtsev et al. 2003), it showed several X-ray outbursts in regular intervals of one to two years. This source was in a quiescent state for a long time—only a couple of X-ray activities were reported by *EXOSAT* in 1984 (Reynolds 1999) and by TTM/COMIS on board *Mir-Kvant* in 1996 (Emelyanov et al. 2000) after its first detection in 1977 August–September by the *Ariel V* all-sky monitor (Kaluzienski & Holt 1997) and *HEAO 1* satellite (Doxsey et al. 1977). This low-mass X-ray binary system is located at R.A. $= 17^{\rm h}46^{\rm m}15\overset{\rm s}{.}61$ and decl. $= -32^{\circ}14'00\overset{''}{.}6$ (Gursky et al. 1978). The mass of this BHC has not yet been dynamically confirmed, although Pétri (2008) predicted that its mass is between $9\,M_{\odot}$ and $13\,M_{\odot}$ with their high-frequency quasi-periodic oscillation (QPO) model. Steiner et al. (2012) have confirmed its distance $D = 8.5 \pm 0.8$ kpc, disk inclination angle $\theta = 75^{\circ} \pm 3^{\circ}$, and spin ($-0.3 < a_{*} < 0.7$, with a 90% confidence).

Recently, in 2010, H 1743-322 was again found to be active in X-rays (Yamaoka et al. 2010) with similar characteristics of

temporal and spectral evolutions as observed in other transient BHCs (Debnath et al. 2008, 2010; Nandi et al. 2012 and references therein). The outburst was observed for a short time period of around two months, and *RXTE* had full coverage of this source on a daily basis. In Debnath et al. (2013, hereafter Paper I), a detailed study of the temporal and spectral properties of the source during its two successive outbursts (2010 and 2011) using the *RXTE* Proportional Counter Array (PCA) archival data are presented. In Paper I, the spectral properties of the source were studied with a combination of conventional thermal (disk blackbody (DBB)) and non-thermal (PL) model components. In order to understand a more realistic picture of the accretion flow dynamics, one needs to study spectral properties with a more physical model (such as TCAF), which would enable one to extract actual physical parameters of the accretion flow. In this paper, we study important physical properties, such as time variation of accretion rates of Keplerian and sub-Keplerian components, shock (when present) location, and strength of the flow, around H 1743-322 during its 2010 outburst by analyzing spectral properties using the TCAF solution. Based on the spectral classification method as defined in Debnath et al. (2014b), four basic spectral states are also observed during the entire period of this outburst, which also form a hysteresis loop, similar to the HID, where different spectral states belong to different branches of the diagram (see Figure 4).

This paper is organized in the following way. In the next section, we discuss observation and data analysis procedures using HEASARC's HeaSoft software package. In Section 3, we present results of spectral analysis using a TCAF-based model *fits* file and variation of different flow parameters with observational results. Finally, in Section 4, we present a brief discussion and make our concluding remarks.

2. OBSERVATION AND DATA ANALYSIS

We analyze data of 26 observational IDs from 2010 August 9 (Modified Julian Day, i.e., MJD = 55417) to 2010 September 30 (MJD = 55469). We carry out data analysis using the FTOOLS software package HeaSoft version HEADAS 6.12 and XSPEC version 12.7. For the generation of source and background ".pha" files and spectral fitting using the TCAF solution, we use the same method as described in Debnath et al. (2014b, hereafter DMC14) and Debnath et al. (2014a, hereafter DCM14).

The 2.5–25 keV PCA background subtracted spectra are fitted with TCAF-based model *fits* file. To achieve the best fit, a Gaussian line of peak energy around 6.5 keV (iron-line emission) is used. For the entire outburst, we keep the hydrogen column density ($N_{\rm H}$) fixed at 1.6×10^{22} atoms cm^{-2} for the absorption model *wabs* and assume a 1.0% systematic error (Paper I). After achieving best fit based on a reduced chi-square value ($\chi^2_{\rm red} \sim 1$), the "err" command is used to find 90% confidence error values for the model fitted parameters. We have not included HEXTE data since the rocking mechanism stopped in 2010; therefore, it is difficult to subtract the background.

For a spectral fit using the TCAF-based model, one needs to supply a total of six input parameters: (1) Keplerian rate ($\dot{m}_d$ in Eddington rate), (2) sub-Keplerian rate ($\dot{m}_h$ in Eddington rate), (3) black hole mass ($M_{\rm BH}$) in solar mass ($M_\odot$) unit, (4) location of the shock (X_s in Schwarzschild radius $r_g = 2GM/c^2$), (5) compression ratio (R) of the shock, and (6) the model normalization value ($norm$) of $R_z^i 2\sin(i)/4\pi D^2$, where R_z is the effective height of the Keplerian disk at the pre-shock region in km, "D" is the source distance in 10 kpc unit and "i" is the disk inclination angle. In order to fit a black hole spectrum with a TCAF model in XSPEC, we generate a model *fits* file (*TCAF.fits*) using theoretical spectra-generating software by varying five input parameters in CT95 code and then including it in XSPEC as a local additive model. A detailed description of the range of input parameters and generation procedure is mentioned in DCM14 and DMC14. In this paper, for the spectra of entire outburst data, we consider the mass of the black hole as $11.4 \pm 1.9\, M_\odot$ (D. Debnath et al. 2014, in preparation).

3. RESULTS

Accretion flow dynamics during an outburst phase of transient BHCs can be explained by a model analysis of spectral and temporal behavior of the source. These behaviors have already been discussed in Paper I, although the analysis was made using a combination of DBB and PL model components that only give the gross properties of the disk. The TCAF-based model goes one step further in extracting the detailed flow parameters, such as two disk rates and shock properties. Furthermore, this makes the boundary of the states more well-defined. Thus, for accretion dynamics, we need to use the TCAF-based model *fits* file.

3.1. Results of the Spectral Data Fitted by the TCAF Solution

Figure 1 shows the variation of X-ray intensities and QPO frequencies, along with the model fitted parameters. In Figure 1(a), the variation of background subtracted from the *RXTE* PCA count rate in the 2–25 keV (0–58 channels) energy band with the day (MJD) is shown. Figures 1(b) and (c) show variations of combined DBB and PL model fitted total spectral flux (flux contributions for DBB and PL model components are calculated by using the convolution model "cflux" technique after fitting spectra with combined model components) in the 2.5–25 keV energy band and the TCAF model fitted total accretion rates (combined Keplerian disk and sub-Keplerian halo rates) in the same energy band. In Figure 1(d), the variation of the accretion rate ratio (ARR; defined to be the ratio of sub-Keplerian halo rate $\dot{m}_h$ and Keplerian disk rate $\dot{m}_d$). Variations of the TCAF model shock locations (X_s) and compression ratios are shown in Figures 1(e) and (f), respectively. Observed QPO frequencies are shown in Figure 1(g). Depending on the variation of the ARR and the nature (shape, frequency, Q value, rms%, etc.) of QPOs (when observed), four different spectral states, i.e., HS, HIMS, SIMS, and SS, could be identified during the entire outburst of H 1743-322 (for details, see DMC14). We observe that the spectral transitions between these states occur approximately on the same day as reported in Paper I (marked with vertical dashed lines in Figures 1 and 2), where spectral classifications were done on the basis of the degree of importance of DBB and PL model components (fluxes) and properties of QPOs. We see that the TCAF model fits well for all four spectral states (model fitted $\chi^2_{\rm red}$ varies $\sim$0.9–2), obeying spectral results of combined DBB and PL. As in DMC14 for the 2010-11 GX 339-4 outburst, we also find two surges in the ARR at the boundaries of hard-intermediate states (HIMS), i.e., from HS to HIMS, during the rising phase or from the HIMS to HS during the declining phase of the outburst transition days. Note that from the TCAF fit, the sum of the accretion rates appears to be almost constant in the HS, both before and after the outburst. At the onset of the SIMS, the total rate rises very sharply. This continues until the SIMS ends. The rate decays monotonically until the end of the HIMS. This is apparent in Figure 2, where we show comparative variations of the combined DBB and PL, the model

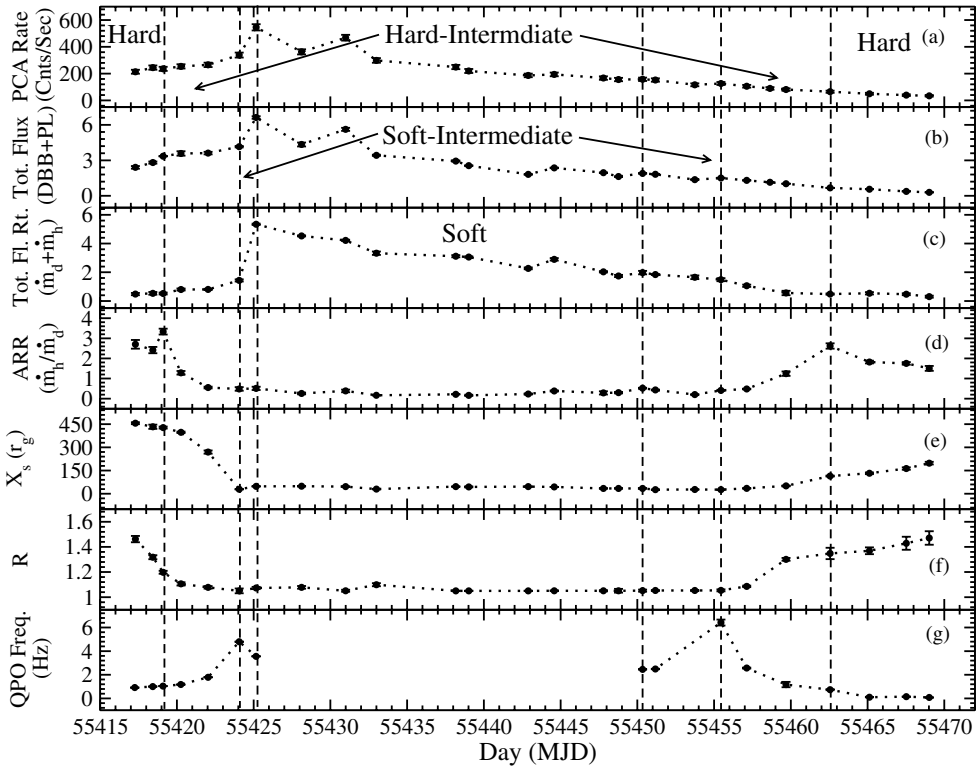

Figure 1. Variation of (a) 2–25 keV PCA count rates (counts s^{-1}), (b) combined disk blackbody (DBB) and power-law (PL) model fitted total spectral flux in the 2.5–25 keV range, (c) TCAF model fitted total accretion rate (sum of Keplerian disk rate $\dot{m}_d$ and sub-Keplerian halo rate $\dot{m}_h$) in the 2.5–25 keV energy band, (d) ARR (i.e., ratio between the halo and disk rates) with day (MJD) for the 2010 outburst of H 1743-322 are shown. In the bottom three panels, variations of the (g) observed QPO frequency in Hz, (e) shock location, and (f) compression ratio are shown. Vertical dashed lines are drawn where we believe transitions of different spectral states have actually taken place.

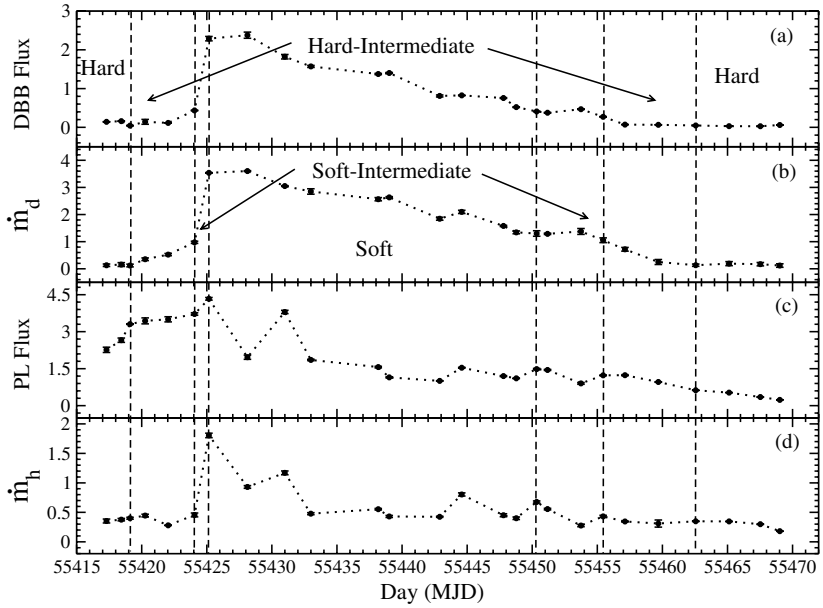

Figure 2. (a) Variations of the combined disk blackbody (DBB) and power-law (PL) model fitted DBB spectral flux in the 2.5–25 keV energy range and (b) variations of the TCAF model fitted Keplerian disk rate ($\dot{m}_d$). Though models are different, these variations appear to be very similar. This is a consistency check for the TCAF solution. In panel (c), the PL spectral flux in the same energy range and in panel (d), the variation of the TCAF model fitted sub-Keplerian halo rate ($\dot{m}_h$) in the same energy band are shown. Though the models are different, the variations of the DBB flux and $\dot{m}_d$ or the PL flux and $\dot{m}_h$ appear to be very similar.

fitted DBB and PL fluxes, and the TCAF model fitted Keplerian disk ($\dot{m}_d$) and sub-Keplerian halo ($\dot{m}_h$) rates with day (MJD). It is important to note that these two variations go hand in hand. We will further discuss Figures 1(e)–(g) later in this paper.

As a further consistency check of TCAF, we ask the following. Could variations of PL flux and $\dot{m}_h$ be similar since the PL component is a result of the scattering of intercepted blackbody photons by the Compton cloud, which is produced by the radiatively inefficient, low angular momentum transonic halo component, according to TCAF? From Figures 2(c) and (d), the similarity is clear. Indeed, the behavior shown in Figure 2 justifies using the more physical model, i.e., TCAF, which

Table 1
2.5–25 keV TCAF Model Fitted Parameters with QPOs

Obs.	Id	UT	MJD	$\dot{m}_d$ ($\dot{M}_{\rm Edd}$)	$\dot{m}_h$ ($\dot{M}_{\rm Edd}$)	ARR	X_s (r_g)	R	QPO (Hz)	χ^2/dof
(1)	(2)	(3)	(4)	(5)	(6)	(7)	(8)	(9)	(10)	(11)
1	X-01-00	09/08/10	55417.29	0.131 ± 0.036	0.353 ± 0.023	2.702 ± 0.218	456.0 ± 6.15	1.462 ± 0.025	0.919 ± 0.004	59.28/42
2[a]	Y-01-00	10/08/10	55418.43	0.156 ± 0.052	0.376 ± 0.021	2.415 ± 0.157	433.1 ± 13.7	1.318 ± 0.016	1.002 ± 0.003	53.66/42
3	Y-02-01	11/08/10	55419.10	0.120 ± 0.051	0.400 ± 0.016	3.333 ± 0.146	427.9 ± 6.56	1.198 ± 0.012	1.045 ± 0.008	62.72/42
4	Y-02-00	12/08/10	55420.26	0.352 ± 0.049	0.445 ± 0.023	1.265 ± 0.090	397.4 ± 4.65	1.106 ± 0.013	1.174 ± 0.002	67.43/42
5[b]	Y-02-03	14/08/10	55422.03	0.524 ± 0.041	0.279 ± 0.014	0.535 ± 0.043	269.6 ± 10.4	1.078 ± 0.010	1.789 ± 0.017	70.23/42
6	Y-03-01	16/08/10	55424.06	0.976 ± 0.042	0.456 ± 0.033	0.467 ± 0.090	29.12 ± 1.56	1.050 ± 0.019	4.796 ± 0.022	42.86/42
7[c]	Y-04-00	17/08/10	55425.16	3.537 ± 0.011	1.805 ± 0.038	0.510 ± 0.083	47.66 ± 1.97	1.073 ± 0.009	3.558 ± 0.024	74.73/43
8	Y-05-00	20/08/10	55428.12	3.602 ± 0.015	0.931 ± 0.023	0.258 ± 0.044	48.56 ± 2.39	1.078 ± 0.011	···	75.56/42
9	Y-07-00	22/08/10	55430.99	3.050 ± 0.016	1.169 ± 0.032	0.383 ± 0.065	46.29 ± 2.26	1.051 ± 0.008	···	65.02/44
10	Y-06-01	24/08/10	55432.99	2.850 ± 0.099	0.477 ± 0.017	0.168 ± 0.012	29.98 ± 1.91	1.099 ± 0.012	···	50.67/42
11	Y-10-00	30/08/10	55438.17	2.565 ± 0.061	0.553 ± 0.013	0.216 ± 0.010	46.02 ± 2.55	1.050 ± 0.002	···	59.59/45
12[d]	Y-11-00	31/08/10	55439.01	2.633 ± 0.028	0.430 ± 0.017	0.163 ± 0.030	44.34 ± 3.23	1.050 ± 0.002	···	69.60/45
13	Y-13-00	03/09/10	55442.89	1.846 ± 0.055	0.425 ± 0.019	0.230 ± 0.026	46.25 ± 0.17	1.050 ± 0.002	···	79.29/45
14	Y-15-00	05/09/10	55444.58	2.098 ± 0.060	0.803 ± 0.027	0.383 ± 0.028	44.09 ± 0.07	1.051 ± 0.003	···	59.33/45
15	Y-18-00	08/09/10	55447.78	1.579 ± 0.022	0.451 ± 0.025	0.286 ± 0.079	34.27 ± 0.06	1.051 ± 0.005	···	34.08/44
16	Y-19-00	09/09/10	55448.77	1.343 ± 0.052	0.399 ± 0.021	0.298 ± 0.037	34.21 ± 0.65	1.051 ± 0.015	···	51.43/45
17	Y-20-00	11/09/10	55450.34	1.301 ± 0.101	0.676 ± 0.018	0.519 ± 0.019	34.21 ± 1.48	1.052 ± 0.008	2.454 ± 0.022	33.70/44
18[e]	Y-20-01	12/09/10	55451.17	1.288 ± 0.024	0.555 ± 0.013	0.431 ± 0.023	26.52 ± 1.16	1.053 ± 0.004	2.489 ± 0.018	43.51/45
19	Y-21-01	14/09/10	55453.74	1.377 ± 0.108	0.276 ± 0.019	0.201 ± 0.026	27.54 ± 1.51	1.053 ± 0.005	···	39.90/45
20	Y-22-01	16/09/10	55455.44	1.052 ± 0.088	0.432 ± 0.018	0.410 ± 0.026	26.40 ± 1.78	1.054 ± 0.008	6.417 ± 0.252	41.57/42
21[f]	Y-23-01	18/09/10	55457.12	0.718 ± 0.069	0.345 ± 0.010	0.480 ± 0.018	34.65 ± 2.24	1.086 ± 0.006	2.569 ± 0.044	42.18/45
22	Y-24-01	20/09/10	55459.68	0.249 ± 0.043	0.310 ± 0.020	1.243 ± 0.110	50.81 ± 2.79	1.301 ± 0.011	1.172 ± 0.226	83.71/42
23[g]	Y-25-01	23/09/10	55462.56	0.133 ± 0.032	0.349 ± 0.015	2.620 ± 0.133	114.4 ± 3.21	1.348 ± 0.045	0.741 ± 0.046	52.27/42
24	Y-28-00	26/09/10	55465.12	0.190 ± 0.034	0.346 ± 0.011	1.820 ± 0.068	132.3 ± 5.63	1.369 ± 0.027	0.102 ± 0.003	41.33/42
25	Y-26-02	28/09/10	55467.52	0.171 ± 0.062	0.299 ± 0.010	1.755 ± 0.064	163.0 ± 7.82	1.429 ± 0.052	0.149 ± 0.005	36.72/42
26	Y-28-01	30/09/10	55469.01	0.120 ± 0.065	0.181 ± 0.013	1.504 ± 0.122	197.9 ± 8.46	1.471 ± 0.054	0.079 ± 0.002	38.72/42

Notes. Here X = 95368-01, Y = 95360-14 indicate the initial part of the observation Ids, and UT date in dd/mm/yy format. $\dot{m}_h$, and $\dot{m}_d$ represent TCAF model fitted sub-Keplerian (halo) and Keplerian (disk) rates in Eddington rate respectively. X_s (in Schwarzchild radius r_g), and R are the TCAF model fitted shock location and compression ratio values respectively. Here, frequency of the principal QPO in Hz are only presented. dof means degrees of freedom of the model fit.

directly gives the intrinsic flow parameters. Furthermore, this shows that the halo rate plays a major role in deciding the spectral properties of the flow. However, at times, the two rates vary independently, as is obvious from Figure 1(d). This will be discussed later in the paper.

In Table 1, the TCAF model fitted parameters, along with frequency of primary observed QPOs (if present), are mentioned. In Figure 3, unabsorbed theoretical model spectra for seven states in the 0.005–1000 keV energy range, selected from different spectral states of the outburst as marked in Table 1, are shown. Note that the relatively harder states clearly show spectral turnover above ∼300 keV. It should also be noted that since the present model of TCAF does not explicitly include magnetic fields, inverse Comptonization of non-thermal photons produced in the post-shock region could not be included; therefore, turnovers that occur at much higher energies in sources such as Cyg X-1 (Zdziarski 2000; Zdziarski et al. 2001; Chakrabarti & Mandal 2006) cannot be fitted with the *fits* file generated using the current TCAF model.

3.2. Evolution of Spectral and Temporal Properties During the Outburst

Detailed temporal and spectral properties of this candidate are discussed by several authors on the basis of whether QPO observation was made or not (Belloni et al. 2005; McClintock et al. 2009; Paper I). However, since we have physical parameters on each day, it may be useful to verify if there is any physical way to differentiate one spectral state from another. In Figures 1(d) and (g), we see that ARR and QPO frequencies vary over time (MJD). The ARR, the total flow/accretion rate ($\dot{m}_d$+$\dot{m}_h$), the shock locations, the compression ratios, etc., in conjunction with QPOs, provide a better understanding of the classification of spectral states.

HS in the rising phase. For the first three days of *RXTE*'s observations (from MJD = 55417.29 to 55419.11), the source was in an HS with increasing total flux and non-thermal PL flux (or, equivalently, the sub-Keplerian halo rate; see Figures 1 and 2). During this phase, the halo rate is increasing faster than the disk rate as the infall time of the halo is shorter than that of the disk. The ARR is monotonically increasing and reached a value of 3.33, the maximum for the entire outburst. QPO frequencies are observed to be increasing monotonically from 0.919 Hz to 1.045 Hz (see Paper I). We define the day of maximum ARR as the transition day from the hard to the hard-intermediate spectral state.

HIMS in the rising phase. The source was in this state for the next ∼5 days after the transition day (MJD = 55419.11). During this phase, the QPO frequency continued to increase monotonically until it reached from 1.045 Hz on MJD = 55419.11 to 4.796 Hz on MJD = 55424.06. The supply of sub-Keplerian matter continued at the same rate, and a part of it was converted to Keplerian matter due to viscous effects, thereby increasing its rate. Consequently, the ARR was decreased. We define the end of the HIMS up to the time when the episode of constant ARR began.

SIMS in the rising phase. The constancy of ARR lasted until the total rate suddenly jumped. Both disk and halo rates, along with the PCA count, rapidly increased until QPOs last. On this day (MJD = 55425.16), the observed QPO frequency (3.558 Hz)

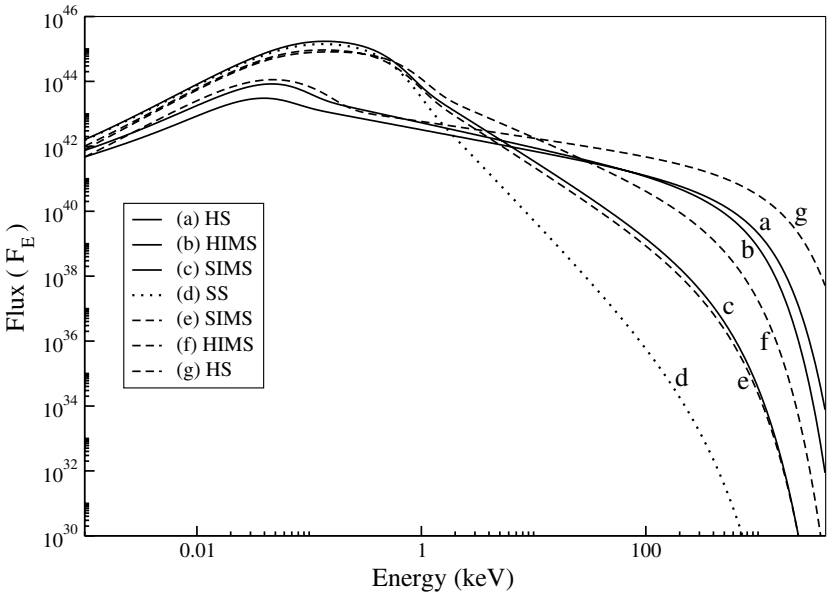

Figure 3. Unabsorbed TCAF model-generated spectra for four different spectral states, which were used to fit the spectra as marked in Table 1. Solid-line plots (a)–(c) are from the rising phase and dashed-line plots (e)–(g) are from the declining phase of the outburst. The dotted plot (d) shows the spectrum of the soft state. Flux (F_E) is in units of photons $\mathrm{cm}^{-2}\ \mathrm{s}^{-1}\ \mathrm{keV}^{-1}$.

did not increase as it previously did. This date of the highest total rate and total PCA counts ended the SIMS and ushered the object to the next state, i.e., the SS.

Soft state. The source is observed at this state for the next $\sim$26 days (up to MJD = 55450.34), where the spectra were mostly dominated by thermal photons. The shock location is very close to the black hole, but is not oscillating, as the resonance oscillation condition is not fulfilled in the presence of rapid cooling. As a result, the QPO is absent. The continuous drainage of Keplerian and sub-Keplerian matter reduced the total rate monotonically, while keeping the ARR roughly constant. This state continues until the drainage is just enough to bring back the resonance condition for the oscillation of the CENtrifugal pressure supported BOundary Layer (CENBOL), whose outer boundary is the shock (see Molteni et al. 1996, hereafter MSC96), and QPOs reappear. The ARR became almost same as that on the date QPO was last observed in the SIMS. On MJD = 55451.17, a state transition is observed.

SIMS in the declining phase. For the following $\sim$5 days, the source was observed in this state. During this period, the total flux (DBB+PL, PCA count rate, and $\dot{m}_d$+$\dot{m}_h$) is almost constant, although, individually, the rates fluctuate. Sporadic QPOs of $\sim$2 Hz are observed during this spectral state. The sporadic phase of a QPO is over on MJD = 55455.44, which signifies the end of this state.

HIMS in the declining phase. On MJD = 55455.44, the HIMS starts. After that, continuous QPOs are observed. The ARR on this day is roughly the same it was on the last day of the HIMS in the rising phase. Initially, the Keplerian disk was drained more rapidly and thus the ARR increased rapidly. Total accretion rate, net PCA count, etc., continued to be drained and The centrifugal pressure-supported shock location started receding (Figure 1(e)) as the incoming flow pressure dropped. As a result, the QPO frequency dropped steadily (see Paper I). On MJD = 55462.56, the maximum ARR (=2.62) of the declining phase is observed, which defines the transition day from the HIMS to the HS

HS in the declining phase. The source is observed in this spectral state until the end of the observation of the 2010 outburst. In this state, the ARR value decreases monotonically from 2.62 to 1.50 and observed QPOs also decrease monotonically from 0.74 Hz to 79 mHz (see Paper I). However, the total rate becomes roughly constant as in the rising phase. The rising phase was observed several days after it began. In the declining phase, the observation continued until the PCA count was much lower than that on the first day of the rising phase. The end of the HS concludes the outburst.

4. DISCUSSIONS AND CONCLUDING REMARKS

We analyzed the spectral properties of the Galactic transient BHC H 1743-322 during its 2010 outburst using the TCAF solution based model after its inclusion as a local additive table model in HEASARC's spectral analysis software package XSPEC. We generate $\sim 4 \times 10^5$ model spectra using the CT95 code to fit with the observational data. Our *fits* file generation procedure is the same as that presented in DMC14. The flow parameters (Keplerian and sub-Keplerian accretion rates) extracted from the TCAF model spectral fit generally match the DBB and PL fluxes (see Figures 1 and 2). Total rate, shock location, and QPOs in different spectral states have been observed to behave as expected. From these quantities, we have a complete physical picture of exactly when spectral state transitions occur.

In Figures 4(a) and (b), we show the variation of derived physical quantities of the flow from our fits. In panel (a), we plot the variation of the PCA count rate as a function of the ratio 1/ARR, and in panel (b), we plot the disk rate as a function of the halo rate for the entire outburst. B, C, D, E, F, and G are points where state transitions take place. In panel (a), segments A–B (black online) and G–H (orange online) show the highest ARR locations; even though the PCA counts are different, the rising phase in A and B (when first caught) is considerably brighter. Segments B and C (red online) and G–F (cyan online) have a roughly similar range of the ARR. The pattern of first horizontal and then vertical variation of the PCA count in the rising phase is reversed in the declining phase. Segments C and D (green online) and E and F (magenta online) are the SIMS occurring roughly at the same ARR value in the rising phase (sharp rise in the PCA

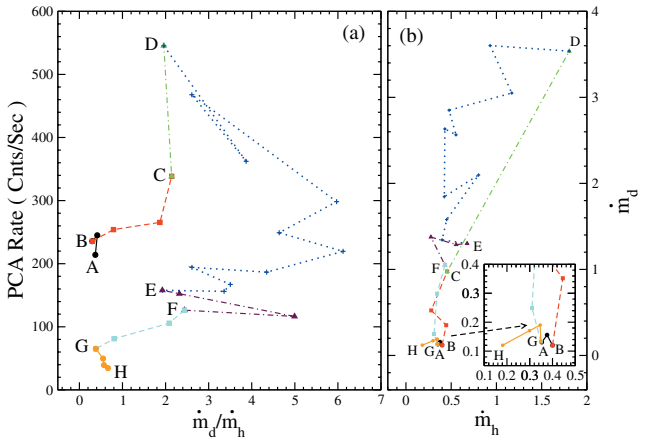

Figure 4. (a) Variation of PCA count rate as a function of 1/ARR and (b) disk rate as a function of halo rate for the entire outburst. Transitions from hard to hard-intermediate (rising) and vice versa (declining) take place when the ARR is at maximum. The soft state begins with the highest value of the individual rates. Duration of the hard-intermediate states in both phases occurs at a similar value of the ARR. For the ARR, $\leqslant$0.5, QPOs are sporadic or absent.

(A color version of this figure is available in the online journal.)

count), but as rapid oscillation in the ARR, although ARR at the edges remain about the same. Segment D and E (blue online) is fluctuating; drainage of the disk and halo being alternately high. Figure 4(b) clearly shows that the two rates are independent, and they do not always increase or decrease together, except in the SS. Indeed, sometimes they are horizontal, and sometimes they are vertical. In these cases, only one component changes to keep the other component constant.

As far as the low-frequency QPO behavior is concerned, it only occurs when the cooling timescale roughly agrees with the infall timescale (MSC96). In HS and HIMS, this is easily achievable as shocks are formed and the Compton cooling timescale is similar to the infall timescale from the shock to the inner edge of the disk. In the SS and the SIMS (when $\dot{m}_d > 1$; see Figure 4(b)), CENBOL is cooled down very rapidly, and shock may or may not be seen. This is true in both the rising and declining phases. Therefore, in the SIMS, QPOs are seen sporadically. When the total rate is at maximum, the SIMS transits to the SS, and the QPO is not seen any more. In the HIMS, $\dot{m}_d$ decreases, while $\dot{m}_h$ remains roughly a similar number. Thus, the ARR increases while going from the HIMS to the HS. The ARR develops a sharp maximum on the day of transition from the HS to the HIMS in the rising phase, and the reverse in the declining phase. This indicates that QPOs are strongly coupled to the cooling properties of the disk.

In the literature, it is in vogue to study the outburst properties using a so-called q-diagram, where hardness is plotted with intensity throughout the outburst (Paper I and references therein). One of the disadvantages of this is that there is no unique definition of hardness and the energy ranges used in the numerator and denominator are rather arbitrary and may be mixtures of soft and Comptonized photons depending on the mass of the black holes. In a TCAF model, we directly extract the accretion rate components and visualize what happens to the object during the outburst (see also Mandal & Chakrabarti 2010). Our direct approach gives more physical insight. Of particular interest is that the ARR plays a vital role in defining the spectral state transitions.

Earlier we showed (DMC14) how spectral state transitions occurred due to the variation of Keplerian and sub-Keplerian rates during the 2010–2011 outburst of the Galactic BHC GX 339-4. We showed the variation of physical parameters, such as accretion rates, ARR, and shock location, and certain behaviors of these parameters at the time of state transitions. From the variation of the Keplerian rate in both these cases, we are now convinced that an outburst is triggered due to a sudden rise in viscosity. The viscous timescale brought much of the Keplerian disk matter into a timescale of about eight days (MJD 55417–55425) in H 1743-322. Drainage took longer as this matter is entrained with a sub-Keplerian halo. It would be interesting to discover if flow dynamics of other outbursting sources also follow a similar trend. The prediction of the QPO frequency from TCAF solution fitted shock parameters (X_s and R) and a comparative study with the POS model solution (Paper I) will be published elsewhere.

S. Mondal acknowledges the support of a CSIR-NET scholarship.

REFERENCES

Belloni, T., Homan, J., Casella, P., et al. 2005, A&A, 440, 207
Cambier, H. J., & Smith, D. M. 2013, ApJ, 767, 46
Chakrabarti, S. K. 1990, Theory of Transonic Astrophysical Flows (Singapore: World Scientific)
Chakrabarti, S. K. 1997, ApJ, 484, 313
Chakrabarti, S. K., & Mandal, S. 2006, ApJL, 642, L49
Chakrabarti, S. K., & Titarchuk, L. G. 1995, ApJ, 455, 623
Debnath, D., Chakrabarti, S. K., & Mondal, S. 2014a, MNRAS, Letters, in press (arXiv:1402.0989) (DCM14)
Debnath, D., Chakrabarti, S. K., Nandi, A., et al. 2008, BASI, 36, 151
Debnath, D., Chakrabarti, S. K., & Nandi, A. 2010, A&A, 520, 98
Debnath, D., Chakrabarti, S. K., & Nandi, A. 2013, AdSpR, 52, 2143 (Paper I)
Debnath, D., Mondal, S., & Chakrabarti, S. K. 2014b, ApJ, submitted (arXiv:1306.3745) (DMC14)
Doxsey, R., Bradt, H., Fabbiano, G., et al. 1977, IAU Circ., 3113, 2
Emelyanov, A. N., Aleksandrovich, N. L., & Sunyaev, R. A. 2000, AstL, 26, 297
Galeev, A. A., Rosner, R., & Vaiana, G. S. 1979, ApJ, 229, 318
Giri, K., & Chakrabarti, S. K. 2013, MNRAS, 430, 2836G
Gursky, H., Bradt, H., Doxsey, R., et al. 1978, ApJ, 223, 973
Haardt, F., & Maraschi, L. 1993, ApJ, 413, 507
Kaluzienski, L. J., & Holt, S. S. 1997, IAU Circ., 3099, 3
Maccarone, T. J., & Coppi, P. S. 2003, MNRAS, 338, 189
Mandal, S., & Chakrabarti, S. K. 2010, ApJL, 710, L147
McClintok, J. E., & Remillard, R. A. 2006, in Compact Stellar X-ray Source, Cambridge Astrophysical Ser., vol. 39, ed. W. Lewin & M. van der Klis (Cambridge: Cambridge Univ. Press), 157
McClintock, J. E., Remillard, R. A., Rupen, M. P., et al. 2009, ApJ, 698, 1398
Molteni, D., Sponholz, H., & Chakrabarti, S. K. 1996, ApJ, 457, 805
Mondal, S., & Chakrabarti, S. K. 2013, MNRAS, 431, 2716
Nandi, A., Debnath, D., Mandal, S., et al. 2012, A&A, 542, 56
Pétri, J. 2008, Ap&SS, 318, 181
Reynolds, P. S. 1999, ApL&C, 38, 425
Revnivtsev, M., Chernyakova, M., Capitanio, F., et al. 2003, ATel, 132, 1
Shakura, N. I., & Sunyaev, R. A. 1973, A&A, 24, 337
Smith, D. M., Heindl, W. A., & Swank, J. H. 2002, ApJ, 569, 362
Soria, R., Wu, K., Hannikainen, D., et al. 2001, in Proc. Workshop, X-Ray Emission from Accretion onto Black Holes, ed. T. Yaqoob & J. H. Krolik, 65
Steiner, J. F., McClintock, J. E., & Reid, M. J. 2012, ApJL, 745, L7
Sunyaev, R. A., & Titarchuk, L. G. 1980, ApJ, 86, 121
Sunyaev, R. A., & Titarchuk, L. G. 1985, A&A, 143, 374
Wu, K., Soria, R., Campbell-Wilson, D., et al. 2002, ApJ, 565, 1161
Yamaoka, K., Negoro, H., Sugizaki, M., et al. 2010, ATel, 2378, 1
Zdziarski, A. A. 2000, in IAU Symp. 195, High Energetic Physical Processes and Mechanisms for Emission from Astrophysical Plasma, ed. P. C. H. Martens, S. Tsuruta, & M. A. Weber (San Francisco, CA: ASP), 153
Zdziarski, A. A., Grove, J. E., Poutanen, J., Rao, A. R., & Vadawale, S. V. 2001, ApJL, 554, L45
Zdziarski, A. A., Lubinski, P., Gilfanov, M., et al. 2003, MNRAS, 342, 355